Communications in Physics, Vol. 35, No. 1 (2025), pp. 75-86

DOI: https://doi.org/10.15625/0868-3166/21873

# Comparison of optical features in nitrobenzene-core photonic crystal fiber with hexagonal and square lattices in the claddings

Trong Dang Van<sup>1</sup>, Bao Tran Le Tran<sup>1</sup>, Ben Chu Van<sup>2</sup> and Lanh Chu Van<sup>1,†</sup>

<sup>1</sup>Department of Physics, Vinh University, 182 Le Duan, Nghe An Province, Vinh City, Vietnam <sup>2</sup>Faculty of Electronic Engineering I, Posts and Telecommunications Institute of Technology, Hanoi, Vietnam

*E-mail*: †chuvanlanh@vinhuni.edu.vn

Received 8 November 2024 Accepted for publication 20 January 2025 Published 6 March 2025

**Abstract.** This paper proposes two novel photonic crystal fibers (PCFs) with a nitrobenzene core, designed using hexagonal and square lattice structures. The characteristics of the PCFs were numerically analyzed in detail and compared to selecting the proposed optimal structure for supercontinuum generation. This study investigates the influence of core diameter ( $D_C$ ) on the characteristics of PCF. The fiber's nonlinear properties are significantly enhanced by varying the core diameter. The hexagonal PCF structures provide flatter dispersion curves and are closer to zero dispersion than the square lattice, which is beneficial for supercontinuum generation. In contrast, the square PCF structures show higher nonlinear coefficients and lower attenuation than the corresponding hexagonal structures. Based on the simulation results, six optimized structures with all-normal and anomalous dispersion were selected to study the characteristics at the pump wavelength. Results indicate that the proposed PCFs exhibit near-zero flat dispersion, low attenuation, and high nonlinearity. The selected optimal structures show potential for efficient supercontinuum generation, enabling broad and highly coherent spectra.

Keywords: photonic crystal fibers (PCFs); hexagonal lattice; square lattice; supercontinuum generation (SCG); dispersion.

Classification numbers: 42.65.Tg; 42.65.Ky; 42.81.Qb.

#### 1. Introduction

In 1996, Russell and his team introduced a groundbreaking optical fiber called photonic crystal fiber (PCF) [1]. PCF, a type of optical fiber leveraging the unique properties of photonic crystals, has gained significant attention due to its superior light transmission capabilities compared to traditional fibers [2–5]. Its cladding features regularly arranged air holes running along the fiber's length. Extensive research has shown that PCF's guiding and optical properties can be tailored by altering its geometry, including adjustments to the core, cladding, air holes, substrate material, or liquid infiltration. This flexibility allows PCFs to be used in various applications, such as sensor fabrication, polarization-maintaining devices, biomedical applications [6–9], and supercontinuum generation [10–15].

Supercontinuum generation (SCG) is one of the applications of PCF that we are particularly interested in researching. SCG is produced when ultra-short optical pulses are introduced into a highly nonlinear medium. To maximize SCG efficiency, PCFs require near-zero, flat dispersion, low attenuation, and a small effective mode area, all of which can be achieved by tuning structural parameters such as lattice constant, air hole size, lattice type, and core material.

In recent years, many research groups have found effective improvements in the optical properties of PCFs filled with liquids with high nonlinear refractive index. Liquid-core PCFs can take full advantage of all the outstanding benefits of high transparency, high nonlinearity, and large thermo-optical coefficients of liquids to optimize the properties of fibers. Planar dispersion with different modes such as all-normal or anomalous dispersion, and low attenuation can be achieved in liquid-core PCFs. Some studies on liquid-core PCFs with a high nonlinear refractive index such as ethanol ( $C_2H_5OH$ ) [16], methanol ( $C_3OH$ ) [17], carbon disulfide ( $C_3OH$ ) [18], chloroform ( $C_3OH$ ) [19], benzene ( $C_3OH$ ) [20], tetrachloroethylene ( $C_3OH$ ) [21], toluene ( $C_3OH$ ) [22] provide planar dispersion, however, the effective mode area is still large, the nonlinear coefficient is relatively low and the attenuation has not yet reached the desired value because these PCFs have the same air hole diameter in the cladding.

To our knowledge, it isn't easy to simultaneously control the characteristic quantities in PCF with the same air-hole diameter in the cladding. These limitations are not beneficial for SCG. In this work, we attempted to construct a novel nitrobenzene-core PCF ( $C_6H_5NO_2$ ) design with different pore sizes to simultaneously achieve the characteristics of flat dispersion, small effective mode area, high nonlinear coefficient, and low attenuation. Nitrobenzene is a good choice because its nonlinear refractive index is higher than that of some commonly used liquids such as carbon tetrachloride ( $CCl_4$ ), tetrachloroethylene, and chloroform. Furthermore, it has only moderate toxicity [23], relatively low attenuation compared to other liquids in terms of nonlinearity, low vapor pressure at room temperature, and easy handling [24].

A large number of works focusing on the study of the characteristics of  $C_6H_5NO_2$ -core PCFs and applying these results to SCG have been carried out in recent years [25–28]. Vu et al. studied the characteristics of hexagonal nitrobenzene core PCFs [25]. The paper showed the possibility of obtaining small effective mode areas, low attenuation, and the resulting dispersion operating in the anomalous dispersion regime. Lanh et al. demonstrated the feasibility of broad and coherent SG spectra in  $C_6H_5NO_2$ -core PCF structures [26]. For the first structure, Lanh et al. obtained SC in the range of 0.8– $1.8~\mu m$ , for the second structure in the range of 0.8– $2.1~\mu m$ , and for the third structure 1.3– $2.3~\mu m$ . Yanchen et al. presented a nitrobenzene core PCF with a high

nonlinear coefficient of 1.43  $W^{-1}$ .m<sup>-1</sup> contributing to the spectral broadening spanning from 1.0 to 2.3  $\mu$ m [27]. Most recently, Wen et al. produced a highly uniform SC in a C<sub>6</sub>H<sub>5</sub>NO<sub>2</sub>-core PCF with eight elliptical air holes in the innermost ring of the cladding [28].

The common feature of previous studies on nitrobenzene core PCFs is that the air holes have equal diameters. Therefore, the values of the characteristic quantities in these reports have not been optimized and have resulted in low SCG performance.

Traditionally, the research on PCFs had mainly focused on three primary lattice structures: circular [9, 10], square [11, 12], and hexagonal [13]. These studies have reported achievements such as high negative dispersion, low confinement loss, and broad bandwidth. However, the optimal PCF design for each lattice type has not been fully evaluated. While some works have examined the impact of fill factor and lattice constant on PCF properties for each lattice type, there is still a need for comprehensive evaluation. For example, Dudley et al. explored the effect of structural parameters on PCF properties for various lattices, the results were not applied to SC generation [14].

Furthermore, many studies have overlooked the influence of varying air hole diameters in different cladding rings on PCF performance. Most previous designs used uniform air hole diameters, optimizing dispersion but not effectively addressing mode area and attenuation [22–26].

To address these limitations, we designed two novel nitrobenzene-core PCFs using hexagonal and square lattices, with varying air hole diameters in the rings to control PCF properties. We varied the air hole diameter in the first ring  $(d_1)$  and the lattice constant  $(\Lambda)$  to study the effect of core diameter on the nonlinear properties of the fibers. Furthermore, in this study, we compared the properties of PCF in two different types of lattices to determine the optimal structure suitable for SCG, which has not been done in previous nitrobenzene studies [25–28].

## 2. Numerical modeling of PCF

In our simulations, the Lumerical Mode Solutions (LMS) software was utilized for numerical analysis. The geometry of the  $C_6H_5NO_2$ -core PCF is depicted in Fig. 1. The fiber is constructed using silica (SiO<sub>2</sub>) as the base material, with nitrobenzene filling the core. This configuration increases the refractive index contrast between the core and cladding, enhancing light confinement within the core. The nitrobenzene is introduced into the core using either a fusion splicer technique [29] or a microfluidic injection system with laser writing technology [30]. The high nonlinear refractive index of nitrobenzene, measured at  $n_2 = 671 \times 10^{-20} \,\mathrm{m^2W^{-1}}$  at 1064 nm [23], is approximately 240 times greater than that of silica [31], making it a superior choice for filling hollow-core PCFs. Its refractive index surpasses other liquids such as CHCl<sub>3</sub> [19], CCl<sub>4</sub> [32–34], C<sub>2</sub>Cl<sub>4</sub> [21,35], and C<sub>7</sub>H<sub>8</sub> [22]. Nitrobenzene, a pale-yellow oil with a characteristic almond scent, is insoluble in water.

Saito et al. [36] demonstrated that the characteristics of PCFs are significantly influenced by the size variations of the air holes within the lattice rings. The size of the holes in the first ring, closest to the core, has a direct impact on dispersion properties, including flatness, the presence of normal or anomalous dispersion, and shifts in the zero-dispersion wavelength (ZDW). The attenuation, on the other hand, is primarily determined by the remaining rings. Based on this idea, we designed two PCF structures (hexagonal and square PCF) and investigated the influence of core diameter ( $D_C$ ) variation on PCF properties. In which, the core diameter was determined using the

formula:

$$D_C = 2\Lambda - 1.1d_1. \tag{1}$$

The air holes in the first ring have a diameter  $(d_1)$  determined by the filling factor  $d_1/\Lambda$ , where  $\Lambda$  is the lattice constant, and  $d_1/\Lambda$  ranges from 0.3 to 0.8, with increments of 0.05. The air holes in the remaining lattice rings have a consistent diameter, corresponding to a filling factor of  $d/\Lambda = 0.95$ . The lattice constants used are  $\Lambda = 1.0 \, \mu \text{m}$ ,  $\Lambda = 1.5 \, \mu \text{m}$ , and  $\Lambda = 2.0 \, \mu \text{m}$ , respectively. Our design introduces new features that minimize attenuation and effective mode area while optimizing chromatic dispersion for improved performance.

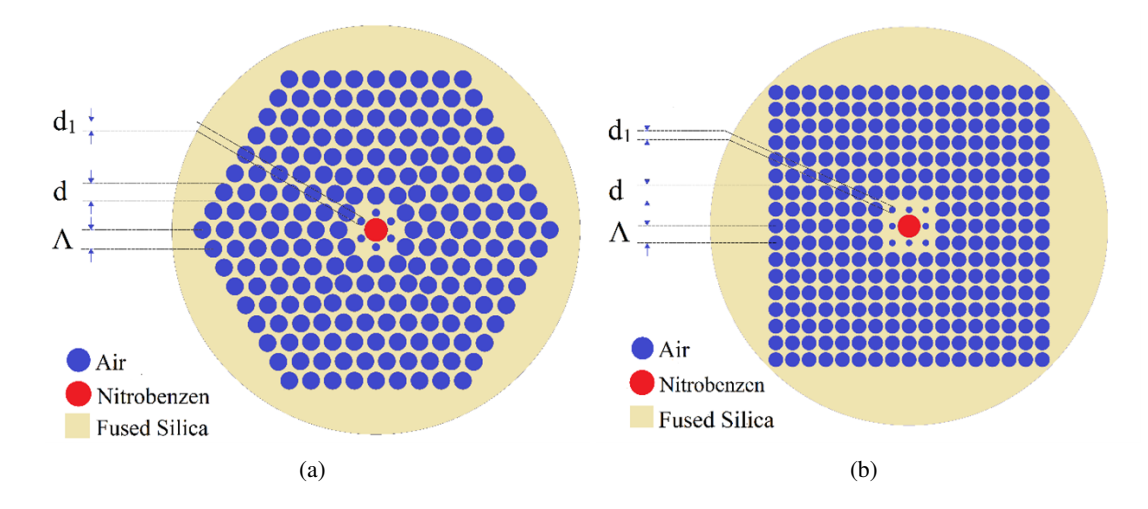


**Fig. 1.** Cross-sectional view of nitrobenzene-core PCF showcasing (a) a hexagonal lattice structure (H-PCF) and (b) a square lattice configuration (S-PCF).

The total dispersion of the fiber arises from both waveguide and material dispersion. This dispersion can be calculated using the following equation:

$$D = -\frac{\lambda}{c} \frac{d^2 \text{Re}[n_{\text{eff}}]}{d\lambda^2},\tag{2}$$

where  $\text{Re}[n_{\text{eff}}]$  refers to the real part of the effective refractive index for the guided mode,  $\lambda$  denotes the pump wavelength in micrometers, and c is the velocity of light in a vacuum [37].

The refractive indices for fused silica and C<sub>6</sub>H<sub>5</sub>NO<sub>2</sub> are computed using the Sellmeier equation, as indicated in:

$$n_{\text{Fused silica}}^{2}(\lambda) = 1 + \frac{0.6694226\lambda^{2}}{\lambda^{2} - 4.4801 \times 10^{-3}} + \frac{0.4345839\lambda^{2}}{\lambda^{2} - 1.3285 \times 10^{-2}} + \frac{0.8716947\lambda^{2}}{\lambda^{2} - 95.341482},$$
(3)

$$n_{Nitrobenzene}^{2}(\lambda) = 1 + \frac{1.30628\lambda^{2}}{\lambda^{2} - 0.02268} + \frac{0.00502\lambda^{2}}{\lambda^{2} - 0.28487},$$
(4)

where the coefficients  $A_i$  and  $B_i$  are material-dependent [38, 39].

The nonlinear coefficient of PCF, expressed in units of  $(W^{-1}km^{-1})$ , is derived using the formula:

$$\gamma = \frac{\omega}{c} \left( \frac{n_2}{A_{eff}} \right) = \frac{2\pi}{\lambda} \left( \frac{n_2}{A_{eff}} \right), \tag{5}$$

where  $\omega$  is the angular frequency, and  $A_{\rm eff}$  is the effective mode area, a key parameter in PCF. The effective mode area is inversely related to the nonlinear coefficient and is calculated by:

$$A_{\text{eff}} = \frac{\left(\int\limits_{-\infty}^{\infty} \int\limits_{-\infty}^{\infty} |E(x,y)|^2 dx dy\right)^2}{\int\limits_{-\infty}^{\infty} \int\limits_{-\infty}^{\infty} |E(x,y)|^4 dx dy},$$
(6)

where E is the electric field amplitude [37].

## 3. Result and Discussion

## 3.1. Dispersion Characteristics

The dispersion characteristics of nitrobenzene-core PCFs with varying core diameter ( $D_C$ ) values are shown in Fig. 2 (a1-a3) H-PCF and (b1-b3) S-PCF.

The variation in dispersion characteristics with respect to core diameter and lattice parameters ( $D_C$  and  $\Lambda$ ) is shown in Fig. 2. The lattice parameters significantly influence the dispersion curves, resulting in a variety of dispersion behaviors. For a small lattice constant ( $\Lambda = 1.0 \,\mu\text{m}$ ), both S-PCF and H-PCF exhibit normal and anomalous dispersion, with one or two zero-dispersion wavelengths (ZDWs). As the  $D_C$  parameter increases, the ZDWs shift towards longer wavelengths.

In the case of anomalous dispersion, a single ZDW is observed for S-PCF when  $D_C = 1.67 \,\mu\text{m}$  and  $D_C = 1.615 \,\mu\text{m}$ . For H-PCF, anomalous dispersion with a single ZDW occurs for the cases  $D_C = 1.67 \,\mu\text{m}$ ,  $D_C = 1.615 \,\mu\text{m}$ , and  $D_C = 1.56 \,\mu\text{m}$ . Notably, the ZDW for S-PCF shifts further into longer wavelengths compared to H-PCF. When  $D_C$  reaches  $1.175 \,\mu\text{m}$  or lower, S-PCF shows anomalous dispersion with two ZDWs, while for H-PCF, this behavior appears at  $D_C = 1.45 \,\mu\text{m}$ . Additionally, the first and second ZDWs of S-PCF are observed at longer wavelengths compared to those of H-PCF.

When  $\Lambda$  exceeds 1.0  $\mu$ m, all-normal dispersion is no longer present, and the dispersion curves shift from normal to anomalous dispersion for both fiber types. Furthermore, for a fixed  $\Lambda$  value ( $\Lambda > 1.0 \mu$ m), the ZDW shifts to longer wavelengths as DC increases. These findings suggest that adjusting the core diameter (the air hole diameter  $d_1$  in the first ring) of the PCF structure allows for precise control over the desired dispersion characteristics.

Dispersion plays a critical role in SCG, and flat dispersion fibers facilitate broader SCG. Therefore, optimizing fiber structures to achieve flat or near-zero dispersion curves with ZDWs matching the pump wavelength is a key objective in dispersion tuning. Different dispersion properties will give different SCG spectral characteristics. When pumping the fiber in the all-normal dispersion regime, the obtained SCG spectrum is broad, flat-topped, low noise, and high coherence. Meanwhile, pumping in the anomalous dispersion regime will obtain a very large SCG spectrum up to several octaves (larger than the all-normal dispersion case) but the spectrum has high noise and low coherence.

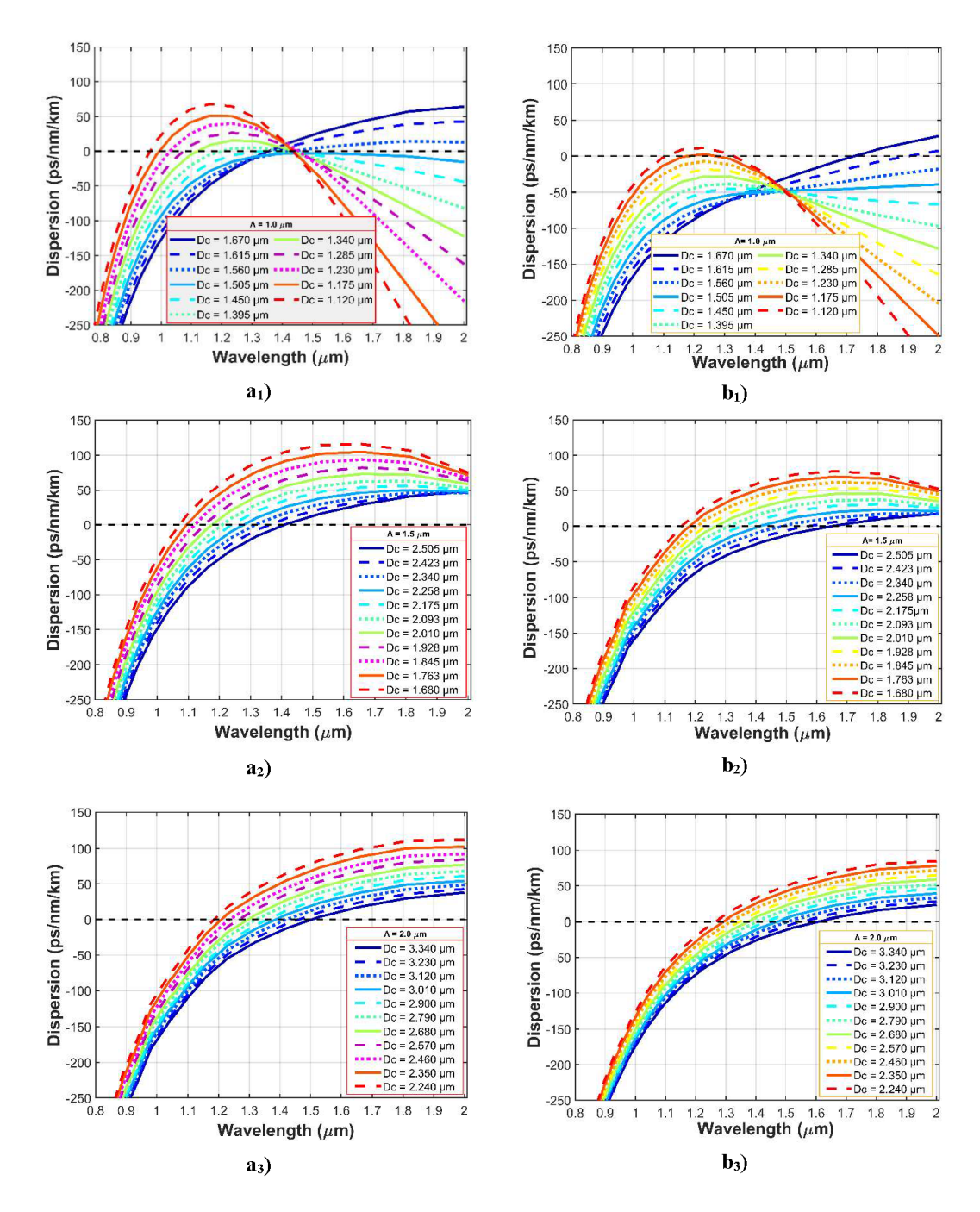


**Fig. 2.** (Color online) The dispersion characteristics of nitrobenzene-core PCFs with varying core diameter ( $D_C$ ) values ( $a_1$ - $a_3$ ) H-PCF and ( $b_1$ - $b_3$ ) S-PCF.

Based on our initial simulations, we propose six optimized fibers with ideal dispersion properties for detailed analysis and orientation for SCG application, as outlined in Table 1.

#	$\Lambda (\mu m)$	$D_C (\mu m)$	Pump wavelength (μm)
HF1	1.0	1.505	1.56
HF2	2.0	3.340	1.55
HF3	1.0	1.395	1.3
SF1	1.0	1.230	1.3
SF2	2.0	3.340	1.61
SF3	1.0	1.175	1.25

**Table 1.** The structural parameters of the proposed PCFs.

The dispersion characteristics of the proposed fibers are presented in Fig. 3. In the hexagonal lattice, the fibers with optimal dispersion are selected as HF1 (1), HF2 (2), and HF3 (3). Meanwhile, SF1 (4), SF2 (5), and SF3 (6) are the fibers with optimal dispersion selected in the square lattice. HF1 and SF1 are pumped in the normal dispersion regime. HF2 and SF2 are pumped in the anomalous dispersion regime with one ZDW. HF3 and SF3 are pumped in the anomalous dispersion regime with two ZDWs. Obviously, in the investigated wavelength region from 0.5 to 2  $\mu$ m, the dispersion profiles of H-PCFs (HF1, HF2, and HF3) are flatter in the larger wavelength region than those of S-PCFs (SF1, SF2, and SF3). In particular, HF1 fiber is the flattest and closest to the horizontal axis, its flatness ranges from 1.3 to 1.8  $\mu$ m, which is very valuable for SCG.

For the H-PCF, fiber HF1 was used for SCG in the all-normal dispersion regime with a pump wavelength of 1.56  $\mu$ m, as this is near the maximum dispersion value, allowing for the broadest SC spectrum. Fiber HF2, operating in the anomalous dispersion regime, is expected to generate a wide SC spectrum at a pump wavelength of 1.55  $\mu$ m, given that its ZDW is closest to the pump wavelength at 1.502  $\mu$ m. Fiber HF3 has a pump wavelength of 1.3  $\mu$ m (ZDW1 = 1.16  $\mu$ m, ZDW2 = 1.32  $\mu$ m), and it also exhibits anomalous dispersion. The dispersion values for fibers HF1, HF2, and HF3 at their respective pump wavelengths are -3.18 ps.nm $^{-1}$ .km $^{-1}$ , 6.22 ps.nm $^{-1}$ .km $^{-1}$ , and 5.34 ps.nm $^{-1}$ .km $^{-1}$ .

For the S-PCF, fiber SF1 operates in the all-normal dispersion regime with a pump wavelength of 1.3 µm, close to the peak dispersion value. Fiber SF2 exhibits anomalous dispersion with a ZDW at 1.607 µm, so a pump wavelength of 1.61 µm was selected for this fiber. Fiber SF3 has a pump wavelength of 1.25 µm (ZDW1 = 1.2 µm, ZDW2 = 1.3 µm). The dispersion values for fibers SF1, SF2, and SF3 at their pump wavelengths are -10.76 ps.nm<sup>-1</sup>.km<sup>-1</sup>, 0.39 ps.nm<sup>-1</sup>.km<sup>-1</sup>, and 2.74 ps.nm<sup>-1</sup>.km<sup>-1</sup>, respectively.

Figure 4 illustrates the attenuation of the fundamental mode as a function of wavelength for the proposed fibers. From Fig. 4, we can see that the attenuation of the proposed S-PCF is lower than that of H-PCF. All six optical fibers exhibit relatively low attenuation values with minimal differences in the wavelength range below 1.5  $\mu$ m. However, for wavelengths between 1.5 and 1.8  $\mu$ m, attenuation increases significantly. The attenuation values at the pump wavelength for fibers HF1, HF2, HF3, SF1, SF2, and SF3 are 6.52 dB/m, 4.92 dB/m, 0.27 dB/m, 6.10 dB/m, 0.17 dB/m, and 0.04 dB/m, respectively. The low attenuation of these fibers is one of the key advantages of this design.

Figures 5 and 6 show the dependence of the effective mode area and the nonlinear coefficient on the wavelength for the fundamental mode of the proposed fibers. The nonlinear coefficient, which is inversely proportional to the effective mode area, is crucial for determining the

input pulse power needed for SCG. A high nonlinear coefficient is beneficial for selecting a low input pulse power in practical applications. At the pump wavelength, the nonlinearity coefficients for fibers SF3, SF1, HF3, HF1, SF2, and HF2 are 2351 W<sup>-1</sup>km<sup>-1</sup>, 2107 W<sup>-1</sup>km<sup>-1</sup>, 1958 W<sup>-1</sup>km<sup>-1</sup>, 1496 W<sup>-1</sup>km<sup>-1</sup>, 441 W<sup>-1</sup>km<sup>-1</sup>, and 471 W<sup>-1</sup>km<sup>-1</sup>, respectively. The small core size and high symmetry of S-PCF result in stronger light confinement in the core, leading to a higher nonlinear coefficient compared to H-PCF. The parameters characterizing the nonlinear properties of the proposed fibers are more optimal than some PCFs infiltrated with other high nonlinear coefficient liquids [19,21,22]. These are also the outstanding advantages of the PCFs in our research.

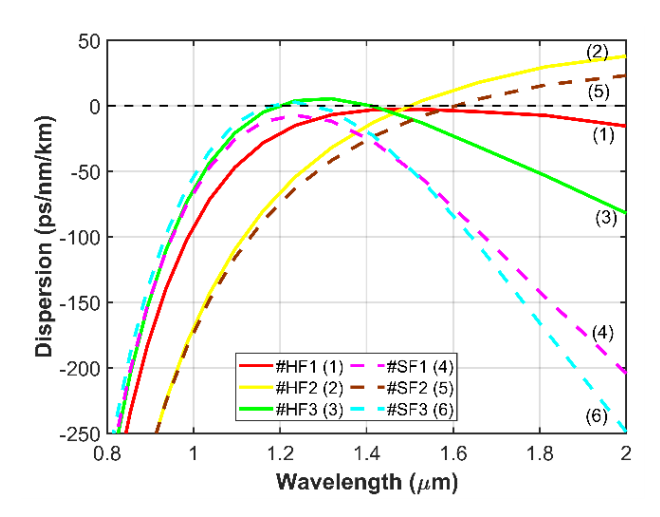


Fig. 3. (Color online) The dispersion properties of the proposed PCFs.

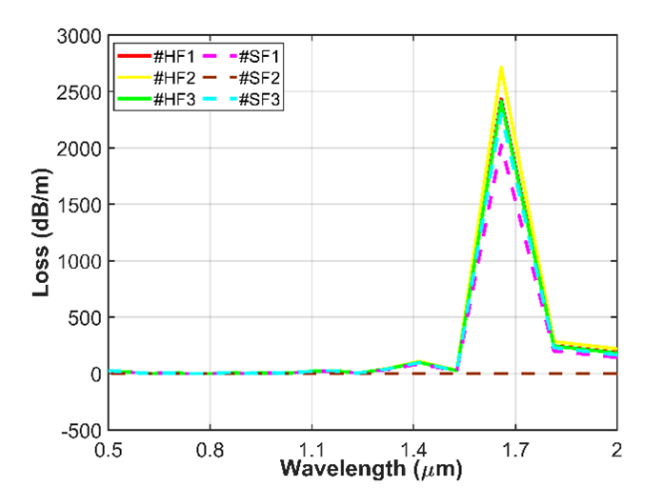


Fig. 4. (Color online) The attenuation properties of the proposed PCFs.

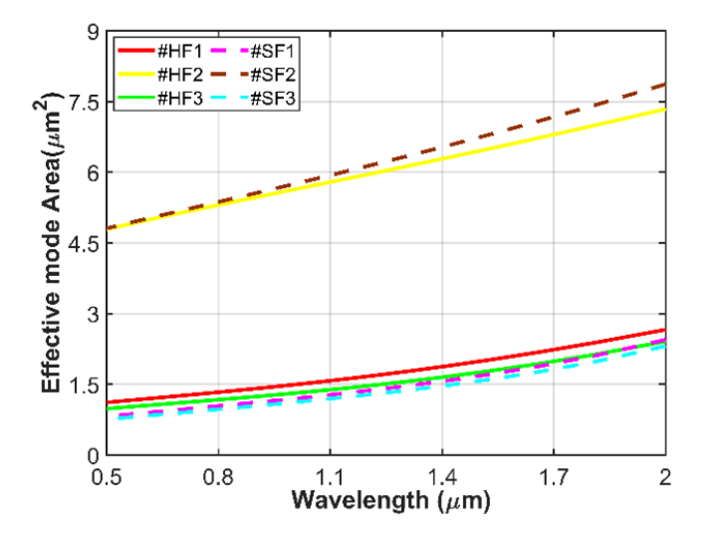


Fig. 5. (Color online) The effective mode area properties of the proposed PCFs.

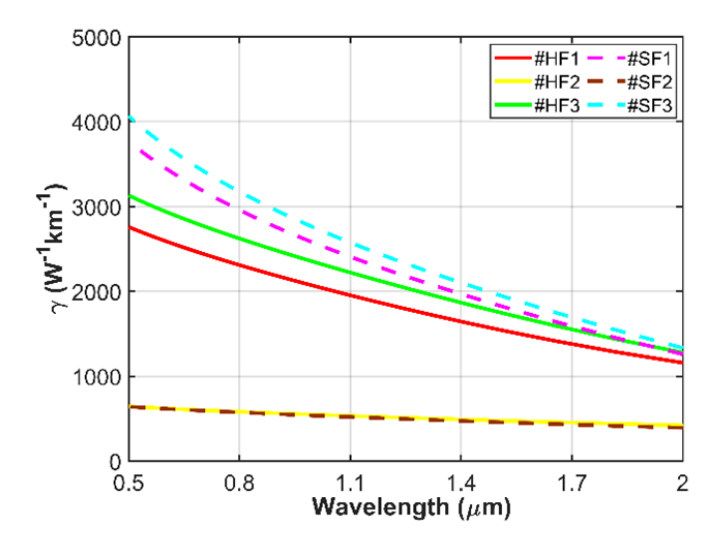


Fig. 6. (Color online) The nonlinear coefficients of the proposed PCFs.

Table 2 presents a comparison between the properties of the proposed fibers and previously reported values. The six fibers introduced in this study demonstrate lower attenuation compared to the works listed in Table 2 [19,21,22]. In the normal dispersion regime, fibers #HF1 and #SF1 exhibit smaller effective mode areas than those previously reported, leading to significantly higher nonlinearities. Specifically, the nonlinearities of fibers #HF1 and #SF2 are 9 times and 12 times greater than those reported in Ref. [22]. Additionally, in the anomalous dispersion regime, the effective mode areas in our study are considerably smaller than those in the compared works.

Table 2.	The v	alue of	quantities	characterized	is calcu	lated at the	pump	wavelength of
the propo	osed Po	CFs.						

Label	Pump λ (μm)	$D$ [ps.(nm.km) $^{-1}$ ]	$A_{\rm eff}  (\mu  {\rm m}^2)$	$\gamma(W^{-1}.km^{-1})$	$L_k \text{ (dB/m)}$
HF1	1.56	-3.18	2.059	1496	6.52
HF2	1.55	6.22	6.538	471	4.92
HF3	1.30	5.34	1.57	1958	0.27
SF1	1.30	-10.76	1.462	2107	6.10
SF2	1.61	0.39	6.978	441	0.17
SF3	1.25	2.74	1.31	2351	0.04
F1 [19] CHCl <sub>3</sub>	1.03	-24.00	1.5	1290	-
F2 [19] CHCl <sub>3</sub>	1.03	7.60	4.48	440	-
F1 [21] C <sub>2</sub> Cl <sub>4</sub>	1.56	-15.00	433.2	156.9	4.0
F2 [21] C <sub>2</sub> Cl <sub>4</sub>	1.56	3.20	16.67	40.79	4.2
F3 [21] C <sub>2</sub> Cl <sub>4</sub>	1.03	-4.85	359.1	189.3	5.3
$I_{0.3}$ [22] $C_7H_8$	1.55	-7.78	7.79	1200	0.4
I <sub>0.3</sub> [22] C <sub>7</sub> H <sub>8</sub>	1.55	-1.19	78.9	-	1.2

These findings indicate that the proposed fibers have optimized dispersion characteristics, making them well-suited for SCG.

## 4. Conclusion

The properties of the newly developed nitrobenzene-core photonic crystal fibers (PCFs) with square and hexagonal lattice designs were thoroughly assessed and compared. Key optical characteristics such as loss, dispersion, effective mode area, and nonlinearity coefficient were extensively analyzed. The impact of lattice type, core diameter, and lattice constant on these properties was explored to optimize both structures. Variations in the fiber geometries resulted in diverse dispersion behaviors, and the ability to finely tune dispersion parameters was achieved by adjusting the core diameter and the lattice constant. We selected six fiber structures with flat all-normal (HF1:  $D_C = 1.505 \,\mu\text{m}$ ,  $\Lambda = 1.0 \,\mu\text{m}$ ; SF1:  $D_C = 1.23 \,\mu\text{m}$ ,  $\Lambda = 1.0 \,\mu\text{m}$ ) and anomalous dispersion, with one (HF2:  $D_C = 3.34 \,\mu\text{m}$ ,  $\Lambda = 2.0 \,\mu\text{m}$ ; SF2:  $D_C = 3.34 \,\mu\text{m}$ ,  $\Lambda = 2.0 \,\mu\text{m}$ ) or two (HF3:  $D_C = 1.395 \,\mu\text{m}$ ,  $\Lambda = 1.0 \,\mu\text{m}$ ; SF3:  $D_C = 1.175 \,\mu\text{m}$ ,  $\Lambda = 1.0 \,\mu\text{m}$ ) zero-dispersion wavelengths to conduct further model analysis of the PCF characteristics. The proposed fibers exhibit low loss, which stands out as a key feature of this work. Although the hexagonal lattice structure displays less uniform dispersion curves than the square lattice, it offers a flatter dispersion curve, closer to zero dispersion, which is highly advantageous for supercontinuum generation. In contrast, the square lattice PCF structure shows higher nonlinearity and lower attenuation compared to their hexagonal counterparts. These simulation results provide valuable insights for designing optical fibers to produce supercontinua with broad, flat, and smooth spectra.

## Acknowledgments

This research is funded by Vietnam National Foundation for Science and Technology Development (NAFOSTED) under grant number 103.03-2023.01.

The author Le Tran Bao Tran was funded by the Master, PhD Scholarship Programs of Vingroup Innovation Foundation (VINIF), code VINIF.2023.TS.133.

## **Conflict of interest**

The authors declare that there are no conflicts of interest.

#### References

- [1] J. C. Knight, T. A. Birks, P. S. J. Russell and D. M. Atkin, *All-silica single-mode optical fiber with photonic crystal cladding*, Opt. Lett. **21** (2020) 1547.
- [2] T. A. Birks, J. C. Knight and P. S. J. Russell, *Endlessly single-mode photonic crystal fiber*, Opt. Lett. **22** (1997) 961.
- [3] J. C. Knight, J. Arriaga, T. A. Birks, A. Ortigosa-Blanch, W. J. Wadsworth and P. S. J. Russell, *Anomalous dispersion in photonic crystal fiber*, IEEE Photon. Technol. Lett. 12 (2000) 807.
- [4] A. Ortigosa-Blanch, J. C. Knight, W. J. Wadsworth, J. Arriaga, B. J. Mangan, T. A. Birks et al., Highly birefringent photonic crystal fibers, Opt. Lett. 25 (2000) 1325.
- [5] V. Finazzi, T. M. Monro and D. J. Richardson, Small-core silica holey fibers: nonlinearity and confinement loss trade-offs, J. Opt. Soc. Am. B 20 (2003) 1427.
- [6] W. J. Wadsworth, A. Ortigosa-Blanch, J. C. Knight, T. A. Birks, T. P. M. Man and P. S. J. Russell, Supercontinuum generation in photonic crystal fibers and optical fiber tapers: a novel light source, J. Opt. Soc. Am. B 19 (2002) 2148.
- [7] S. Dupont, C. Petersen, J. Thøgersen, C. Agger, O. Bang and S. R. Keiding, *Ir microscopy utilizing intense supercontinuum light source*, Opt. Express **20** (2012) 4887.
- [8] K. Ke, C. Xia, M. N. Islam, M. J. Welsh and M. J. Freeman, Mid-infrared absorption spectroscopy and differential damage in vitro between lipids and proteins by an all-fiber-integrated supercontinuum laser, Opt. Express 17 (2009) 12627.
- [9] C. R. Petersen, N. Prtljaga, M. Farries, J. Ward, B. Napier, G. R. Lloyd et al., Mid-infrared multispectral tissue imaging using a chalcogenide fiber supercontinuum source, Opt. Lett. 43 (2018) 999.
- [10] B. Liu, M. Hu, X. Fang, Y. Wu, Y. Song, L. Chai et al., High-power wavelength-tunable photonic-crystal-fiber-based oscillator-amplifier-frequency-shifter femtosecond laser system and its applications for material microprocessing, Laser Phys. Lett. 6 (2009) 44.
- [11] T. Udem, R. Holzwarth and T. W. Hänsch, Optical frequency metrology, Nature 416 (2002) 233.
- [12] R. Buczynski, D. Pysz, R. Stepien, A. J. Waddie, I. Kujawa, R. Kasztelanic et al., Supercontinuum generation in photonic crystal fibers with nanoporous core made of soft glass, Laser Phys. Lett. 8 (2011) 443.
- [13] J. K. Ranka, R. S. Windeler and A. J. Stentz, Visible continuum generation in air-silica microstructure optical fibers with anomalous dispersion at 800 nm, Opt. Lett. 25 (2000) 25.
- [14] J. M. Dudley, L. Provino, N. Grossard, H. Maillotte, R. S. Windeler, B. J. Eggleton et al., Supercontinuum generation in air-silica microstructured fibers with nanosecond and femtosecond pulse pumping, J. Opt. Soc. Am. B 19 (2002) 765.
- [15] K. D. Xuan, L. C. Van, Q. H. Dinh, L. V. Xuan, M. Trippenbach and R. Buczynski, *Dispersion characteristics of a suspended-core optical fiber infiltrated with water*, Appl. Opt. **56** (2017) 1012.
- [16] L. T. B. Tran, N. T. Thuy, V. T. M. Ngoc, L. C. Trung, L. V. Minh, C. L. Van et al., Analysis of dispersion characteristics of solid-core pcfs with different types of lattices in the claddings, infiltrated with ethanol, Photonics Lett. Pol. 12 (2020) 106.
- [17] P. Chauhan, A. Kumar and Y. Kalra, Supercontinuum generation in a hollow-core methanol-silica based photonic crystal fiber: computational model and analysis, in Proc. SPIE 11498, Photonic Fiber and Crystal Devices: Advances in Materials and Innovations in Device Applications XIV, p. 114980T, 2020, DOI.
- [18] A. Sharafali, A. K. S. Ali and M. Lakshmanan, *Modulation instability induced supercontinuum generation in liquid core suspended photonic crystal fiber with cubic-quintic nonlinearities*, Phys. Lett. A **399** (2022) 127290.

- [19] C. V. Lanh, V. T. Hoang, V. C. Long, K. Borzycki, K. D. Xuan, V. T. Quoc et al., Optimization of optical properties of photonic crystal fibers infiltrated with chloroform for supercontinuum generation, Laser Phys. 29 (2019) 075107.
- [20] C. V. Lanh, V. T. Hoang, V. C. Long, K. Borzycki, K. D. Xuan, V. T. Quoc et al., Supercontinuum generation in benzene-filled hollow-core fibers, Opt. Eng. 60 (2021) 116109.
- [21] H. V. Le, V. T. Hoang, H. T. Nguyen, V. C. Long, R. Buczyński and R. Kasztelanic, Supercontinuum generation in photonic crystal fibers infiltrated with tetrachloroethylene, Opt. Quant. Electron. 53 (2021) 187.
- [22] L. C. Van, A. Anuszkiewicz, A. Ramaniuk, R. Kasztelanic, K. X. Dinh, M. Trippenbach et al., Supercontinuum generation in photonic crystal fibers with core filled with toluene, J. Opt. 19 (2017) 125604.
- [23] Y. Xu, X. Chen and Y. Zhu, *High sensitive temperature sensor using a liquid-core optical fiber with small refractive index difference between core and cladding materials*, Sensors 8 (2008) 1872.
- [24] R. L. Sutherland, D. G. McLean and S. Kirkpatrick, Handbook of Nonlinear Optics. CRC Press, Boca Raton, 2003.
- [25] V. T. Quoc, C. T. G. Trang, L. V. Minh, N. T. Thuy, N. T. H. Phuong, D. Q. Khoa et al., Feature properties of photonic crystal fiber with hollow core filled by nitrobenzene, Comm. Phys. 30 (2020) 331.
- [26] L. C. Van, V. T. Hoang, V. C. Long, K. Borzycki, K. D. Xuan, V. T. Quoc et al., Supercontinuum generation in photonic crystal fibers infiltrated with nitrobenzene, Laser Phys. 30 (2020) 035105.
- [27] G. Yanchen, Y. Jinhui, W. Kuiru, W. Haiyun, C. Yujun, Z. Xian et al., Generation of supercontinuum and frequency comb in a nitrobenzene-core photonic crystal fiber with all-normal dispersion profile, Opt. Commun. 481 (2021) 126555.
- [28] J. Wen, L. Bozhi, Q. Weijun, S. Wei, H. Chenyao and X. Keyu, High coherent supercontinuum generation in nitrobenzene liquid-core photonic crystal fiber with elliptical air-hole inner ring, Opt. Quant. Electron. 54 (2022) 817
- [29] V. T. Hoang, R. Kasztelanic, A. Anuszkiewicz, G. Stepniewski, A. Filipkowski, S. Ertman et al., All-normal dispersion supercontinuum generation in photonic crystal fibers with large hollow cores infiltrated with toluene, Opt. Mater. Express 8 (2018) 3568.
- [30] M. Vieweg, T. Gissibl, S. Pricking, B. T. Kuhlmey, D. C. Wu, B. J. Eggleton et al., Ultrafast nonlinear optofluidics in selectively liquid-filled photonic crystal fibers, Opt. Express 18 (2010) 25232.
- [31] H. V. Le, V. T. Hoang, Q. D. Ho, H. T. Nguyen, N. V. T. Minh, M. Klimczak et al., Silica-based photonic crystal fiber infiltrated with 1,2-dibromoethane for supercontinuum generation, Appl. Opt. 60 (2021) 7268.
- [32] Q. H. Dinh, J. Pniewski, H. L. Van, A. Ramaniuk, V. C. Long, K. Borzycki et al., Optimization of optical properties of photonic crystal fibers infiltrated with carbon tetrachloride for supercontinuum generation with subnanojoule femtosecond pulses, Appl. Opt. 57 (2018) 3738.
- [33] V. T. Hoang, R. Kasztelanic, G. Stepniewski, K. D. Xuan, V. C. Long, M. Trippenbach et al., Femtosecond supercontinuum generation around 1560 nm in hollow-core photonic crystal fibers filled with carbon tetrachloride, Appl. Opt. 59 (2020) 3720.
- [34] V. T. Hoang, R. Kasztelanic, A. Filipkowski, G. Stepniewski, D. Pysz, M. Klimczak et al., Supercontinuum generation in an all-normal dispersion large core photonic crystal fiber infiltrated with carbon tetrachloride, Opt. Mater. Express 9 (2019) 2264.
- [35] L. C. Van, H. V. Le, N. D. Nguyen, N. V. T. Minh, Q. H. Dinh, V. T. Hoang et al., Modeling of lead-bismuth gallate glass ultra-flatted normal dispersion photonic crystal fiber infiltrated with tetrachloroethylene for high coherence mid-infrared supercontinuum generation, Laser Phys. 32 (2022) 055102.
- [36] K. Saitoh, M. Koshiba, T. Hasegawa and E. Sasaoka, Chromatic dispersion control in photonic crystal fibers: application to ultra-flattened dispersion, Opt. Express 11 (2003) 843.
- [37] G. P. Agrawal, Nonlinear Fiber Optics. Academic Press, Elsevier, 2013.
- [38] C. Z. Tan, Determination of refractive index of silica glass for infrared wavelengths by ir spectroscopy, J. Non-Cryst. Solids 223 (1998) 158.
- [39] S. Kedenburg, M. Vieweg, T. Gissibl and H. Giessen, *Linear refractive index and absorption measurements of nonlinear optical liquids in the visible and near-infrared spectral region*, Opt. Mater. Express 2 (2012) 1588.